Edge transport barrier in JET hot ion H modes

H.Y. Guo*, P.J. Lomas, V.V. Parail, P. Andrew, B. Balet, G.D. Conway,
B. De Esch, C.W. Gowers, M.G. von Hellermann, G.T.A. Huysmans,
T.T.C. Jones, M. Keilhacker, R.W.T. König, A. Maas, F.B. Marcus,
G.F. Matthews, M.F.F. Nave[a], F.G. Rimini, R.J. Smith, M.F. Stamp,
A. Taroni, P.R. Thomas, K.-D. Zastrow
JET Joint Undertaking,
Abingdon, Oxfordshire, United Kingdom

[a] Associação Euratom/IST,
    Lisbon, Portugal

Abstract. The effects of changing beam and plasma species on the edge transport barrier are investigated for ELM-free hot ion H mode discharges from the recent DT experiments on JET. The measured pressure at the top of the pedestal is higher for mixed deuterium and tritium and pure tritium plasmas over and above the level measured in pure deuterium plasmas at the same heating power. The pedestal pressure increases with beam tritium concentration for mixed deuterium–tritium beam injection into deuterium plasmas where the measured edge tritium concentration remains low. Alpha heating plays a significant role in the core of such plasmas, and the possible impact on the edge is discussed together with possible direct isotopic effects. Heuristic models for the transport barrier width are proposed, and used to explore a wider range of edge measurements including full power DD and DT pulses. This analysis supports the plasma current and mass dependence for a barrier width set by the orbit loss of either thermal or fast ions, though it does not unambiguously distinguish between them. The fast ion hypothesis could well account for some of the JET observations, though more theoretical work and direct experimental measurement would be required to confirm this. An ad hoc model for the power loss through the separatrix, $P_{loss} \propto n_{edge}^2 Z_{eff,edge} I_p^{-1}$, is proposed based on neoclassical theory, a ballooning limit to the edge gradient and a barrier width set by the poloidal ion gyroradius. Such a model is compared with experimental data from JET. In particular, the model ascribes the systematic difference in loss power between the Mark I and Mark II divertors to the change in the measured Z_{eff}. This change in Z_{eff} is consistent with the observed change in impurity production, which is described in some detail, together with a possible explanation provided by the temperature dependence of chemical sputtering.

1. Introduction

Hot ion ELM-free H mode discharges have delivered the world record for fusion power (16.1 MW) [1] and have clearly demonstrated alpha particle heating [2] during the recent DT experiments (DTE1) on JET. The characteristic feature of this regime is a low initial (target) plasma density, coupled with low levels of neutral recycling. The low target density, in combination with high power neutral beam heating, allows the ions to be decoupled from the electrons and thus maximizes fusion performance. Low levels of recycling, highly shaped plasmas and high plasma current are necessary to maximize both the ELM-free period and the fusion performance [3, 4].

A key feature of the hot ion H mode (as well as other H mode plasmas [5]) lies in its edge transport barrier. Firstly, the edge transport barrier controls the energy losses through the separatrix. It has been observed that the confinement, normalized to the ELM-free H mode scaling prediction (ITER 93-H), rises approximately linearly with time, during the ELM-free phase, up to a factor ∼1.8 [6] in the hot ion H mode plasmas. This observation is consistent with predictions from an empirical model, proposed by Parail, Cherubin and others [6, 7], which requires the anomalous heat transport across the edge transport barrier region to be significantly reduced or suppressed so that the remaining transport approaches the level of ion neoclassical thermal conductivity. Assuming that the width of the edge transport barrier is determined by the ion poloidal banana width, the neoclassical model predicts that

---

the loss power through the separatrix is given by $P_{loss} \propto n_{edge}^2 Z_{eff,edge} I_p^{-1}$, where I_p is the plasma current, and n_{edge} and $Z_{eff,edge}$ are the electron density and Z_{eff} at the edge. Secondly, the edge transport barrier controls the edge ballooning and kink instabilities which are driven by the edge pressure gradient (ballooning mode directly and kink mode via bootstrap current). Assuming that the pressure gradient within the edge transport barrier is constant, both the energy flux through the separatrix and the maximum plasma pressure at the top of the barrier are controlled by the width of the edge transport barrier. There has been a variety of theoretical proposals about the possible scaling for the width of the edge transport barrier since the discovery of H modes [8–16]. However, due to inadequate experimental information on the edge region, which exhibits steep gradients, it is still not clear which mechanisms control the width of the edge transport barrier. Recently, it has been suggested that in some cases the width of the edge transport barrier can be controlled by the orbit losses of fast ions from NBI [17].

In outline the present article is as follows. In Section 2 we report the experimental observations of the isotopic effects on the edge transport barrier in the hot ion H modes from the DTE1 campaign and show the evidence for the role of fast particles. In Section 3 we first describe the models for the width of the edge transport barrier, followed by the experimental scaling of the edge transport barrier width with different model assumptions. In Section 4 the loss power is compared with the predictions from the neoclassical transport model, based on the width scaling for the edge transport barrier. In Section 5 we attempt to explain the difference in loss power between the Mark I and Mark II divertors in terms of the neoclassical heat transport within the edge transport barrier, and hence demonstrate the significance of edge recycling and impurity production for the hot ion regimes. The summary and conclusions follow in Section 6.

2. Isotopic effects on edge transport barrier

2.1. Edge pressure and ELM-free period in DD and DT

While it is affected by a variety of MHD phenomena, such as the sawteeth or the outer modes [18], the performance phase of the hot ion H mode is eventually terminated by the occurrence of a giant type I

ELM [19]. It has been shown that the type I ELM [20] is usually associated with ideal ballooning modes [21–23]. This is consistent with the observations of the hot ion modes at different plasma currents, which show that the giant (type I) ELM occurs as the edge pressure gradient approaches the ballooning instability limit [24].

At JET the edge pressure, including both electron and ion pressure, i.e. $p_{edge} = e(n_e T_e + n_i T_i)_{edge}$, is measured at $R = 3.75$ m, corresponding to $r/a \approx 0.9$, at the top of the pedestal, inside the steep gradient region. The edge electron density, n_{edge}, is a line average, determined by the edge channel of the interferometer. The edge electron temperature, $T_{e,edge}$, is a local measurement at the same position, obtained from ECE. The ion pressure at the edge is measured by CX diagnostics, taking into account impurity dilution.

In order to illustrate the first comparison between DD and DT, we have chosen a pair of discharges with the same neutral beam heating power, plasma current, toroidal field and configuration and where the deuterium reference specifically included ICRF heating to simulate the alpha heating in the DT pulse. Figure 1 shows the evolution of the edge pressure, p_{edge}, together with the other plasma parameters at the edge for a hot ion H mode in DD (pulse 41068), in comparison with that in DT with ∼60% tritium in the discharge (pulse 42856). Both pulses have the same plasma current (3.8 MA) and toroidal magnetic field (3.4 T). The total heating power supplied by the neutral beams is also the same (∼10 MW), but for the DT pulse the neutral beams consist of the same isotopic composition as in the plasma. In addition, up to 2 MW of ICRF heating is applied in the DD pulse to simulate the alpha heating which would occur in DT.

Note that in this pair of discharges, the ICRF in the DD pulse reproduces the core electron heating due to alpha particles in the DT pulse, as shown in Ref. [2], and, with matched ion and electron heat inputs. Figure 1 shows that the rates of rise of edge density, edge electron temperature and edge ion temperature are also well matched. However, these continue to rise for longer in the DT case, where the ELM occurs later, such that the edge pressure at the ELM is higher. The difference in pedestal pressure (about 25%) between these discharges is more than twice the uncertainty in the measurement (about 10%), and as such provides the first evidence for a significant isotopic effect. In order to exclude other effects, such as recycling, shot to shot reproducibility,
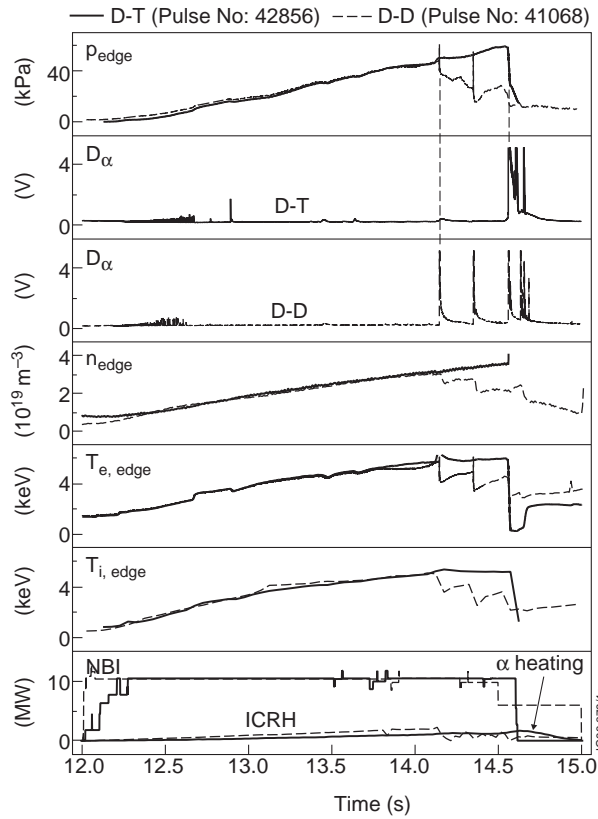
Figure 1. Time traces of two comparable hot ion H modes (10 MW, 3.8 MA, 3.4 T) performed in DD (pulse 41068) and in DT (pulse 42856) plasmas illustrating the changes in the edge pressures. Data shown are the edge pressure, D_α emissions from the strike zone in the outer divertor, the electron density, the electron temperature, the ion temperature and the additional heating power.

MHD and power balance, which might contribute to the observed difference, a wider range of DD plasmas is now discussed.

Comparison of DD and DT discharges at the same beam power, but without simulating the effect of alpha heating, shows that the rise of the edge pressure in DD is generally slower than that in DT. This results in ELM-free periods as long as those in the DT cases. However, it is possible that this arises from differences in recycling, and according to how the walls were pre-loaded with DT. To investigate the effect of recycling, independent of isotopic effects, Fig. 2 compares the evolution of the edge parameters for two DD discharges with different recycling levels. The two discharges have the same neutral beam heating power as the discharges shown in Fig. 1. As can be seen, at higher recycling level, the edge density rises faster, but the rise in both electron and
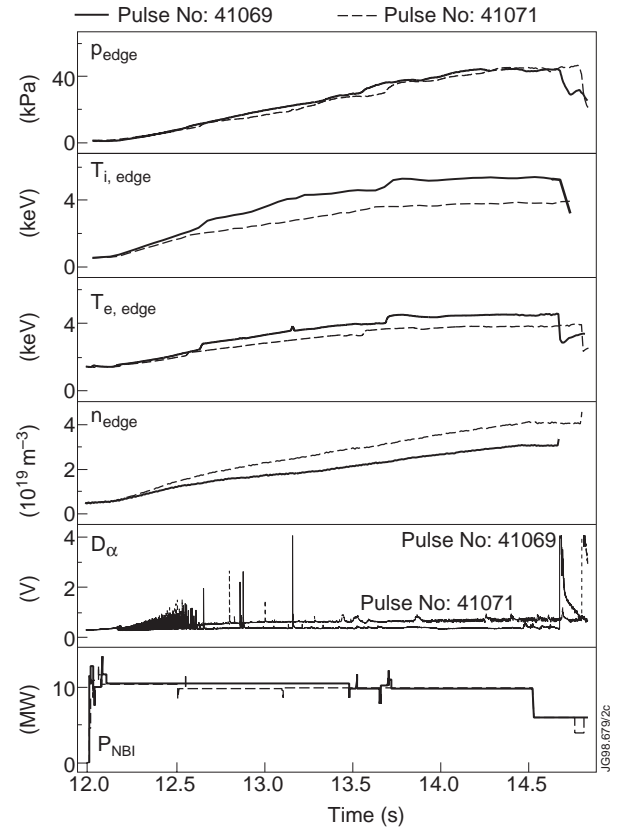

Figure 2. Evolution of the edge pressure, the ion temperature, the electron temperature and the electron density of two DD hot ion H modes with the same neutral beam heating (10 MW), but with different recycling conditions, as indicated by the D_α emissions.

ion temperature at the edge is reduced. As a result, the evolutions of edge pressure are similar for the two discharges, reaching similar edge pressure values at the onset of the giant ELM. Notice that the maximum pressures obtained in these two discharges are comparable to that in the DD alpha particle simulation discharge (with ICRH) (Fig. 1) in spite of very different recycling conditions. The ELM-free periods in the neutral beam only DD discharges are longer, due to the slower rate of rise in edge pressure, compared with the alpha particle simulation pulse.

A large number of the DD discharges with different edge recycling conditions were carried out prior to the DT campaign. It is found that with similar plasma current, the maximum edge pressure in DD is lower than that obtained in DT. In particular, a survey over the entire 10 MW neutral beam heated DD and DT hot ion H modes (over 30 discharges) shows that the maximum edge pressure at the onset of the giant ELM varies between about 40
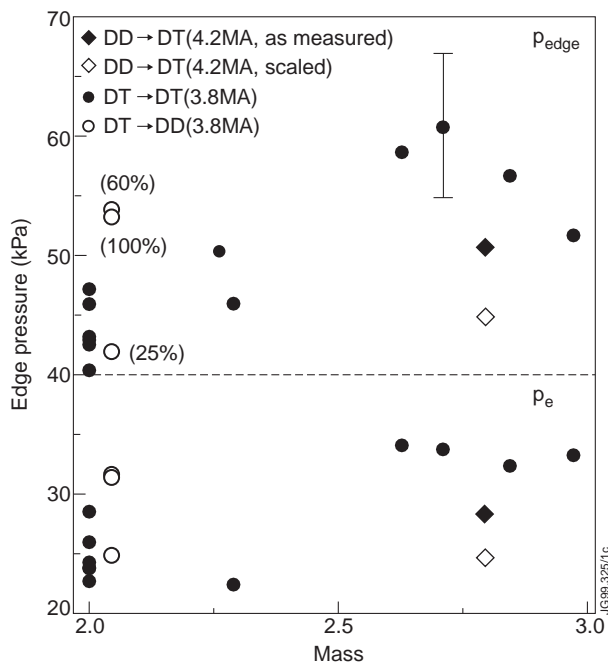
Figure 3. Edge pressure at the onset of ELMs versus edge isotopic composition for a series of 3.8 MA/3.4 T hot ion H modes with NBI power of ∼10 MW, in which the isotopic composition of the NBI beam particle source is closely matched to that in the background plasma. Also shown are the data from the discharges with a pure deuterium background plasma and tritium fast particles from the neutral beams, as well as the result from a discharge at 4.2 MA/3.6 T with pure deuterium beams whilst the gas and walls were tritium rich.

and 47 kPa, whilst the highest value obtained in the comparable DT discharges is about 60 kPa. The data for some typical discharges are shown in Fig. 3, for comparison with DT discharges, and will be further discussed in Section 2.2.

It is well known that the hot ion H mode plasma is very rich in the different types of MHD phenomena such as sawteeth and outer modes [19], which might sometimes interfere with ELMs and thus affect both the edge pressure and the ELM-free period. The simplest example is a sawtooth crash which redistributes the plasma pressure and can lead to a sudden increase in the edge pressure followed by a prompt ELM. Since our assumption is that the cause of type I ELMs is the ballooning instability, the edge pressure should be measured as close to the onset of the ELMs as possible. The outer modes (driven by the external ideal kink instability [18]), like ELMs, are also edge localized phenomena. If they are

localized in the plasma inside the edge transport barrier, we might expect an increase of the edge pressure, which should be taken into account while evaluating the edge pressure. However, we sometimes observe a decrease in the edge pressure due to the outer modes. This might happen in a case where the outer modes are localized within the barrier outside the position of our edge measurements (at $r/a \approx 0.9$). Such outer modes could cause a local perturbation of the pressure gradient within the barrier region, and hence trigger a relatively small ELM. In this case our measurements are not reliable and are therefore excluded from analysis. In addition, some small benign ELMs could occur before the edge pressure reaches a critical level. There are a number of phenomena which might cause these premature ELMs, such as UFOs. In the present article, we will not discuss these small ELMs and concentrate on the giant ELM which destroys the edge transport barrier and terminates the high performance phase of the hot ion H modes.

If the pedestal pressure limit were set by power balance arguments, then we might expect to see the largest variation in pedestal height by comparing low power data with data which has the maximum neutral beam and ICRF heating. The high power data (with up to 20 MW of neutral beam heating and up to 8 MW of ICRF) show the highest pedestal pressures observed in DD plasmas of up to 52 kPa, and no clear variation according to the proportion of ion or electron heating. This value is still smaller than the low power DT example shown. It seems unlikely, therefore, that the difference between the two discharges of Fig. 1 could be readily explained by a difference in the power balance caused by differences between ICRH and alpha heating. We shall return to this point in Section 2.2. The high power discharges, in both DD and DT, are discussed in more detail in Section 3.3 and Ref. [25].

To summarize, in this section a difference in pedestal pressure has been demonstrated between DD and DT plasmas which is larger than measurement error or shot to shot reproducibility. Large changes in the power balance could affect the pedestal but the effect must be very small. Outer mode activity can also limit the pedestal height and these cases have been eliminated from our analysis. It is concluded that an isotopic effect manifests itself as an increase in the limiting edge pressure at the giant ELM in the DT plasma of Fig. 1 compared with that in DD. In the next section we will turn our attention to the remainder of the low power DT data.

2.2. The low power DT experiments

In this section we introduce the complete set of low power DT data in the ELM-free regime, describe the main features in the pedestal measurements and explore the possible interpretations of these data in terms of alpha heating, isotopic effects and the influence of fast particles.

The low power data set consists of three separate experiments. The first of these is the alpha heating experiment described in Ref. [2]. These discharges were performed at 3.8 MA/3.4 T with almost constant neutral beam heating power (10 MW) and little variation in the particle source. The tritium concentration was varied from 0 to nearly 100% by simultaneous control of the gas and neutral beam fuelling. The vacuum vessel walls and divertor target were loaded with the required DT mixture to ensure that the recycling composition was as close as possible to that of the gas and NBI sources. The edge T/D composition was measured by tritium and deuterium measurements, neutral particle analysis and Penning spectroscopy in the subdivertor volume [1] and reached 97% at the extreme point of the scan. The second experiment to be described was the mixture experiment [1], which was actually performed before any significant contamination of the walls and divertor target with tritium. Again 3.8 MA/3.4 T and 10 MW of NBI were used, but in this case only the beam tritium concentration was varied (25, 60 and 100%), whilst the gas fuelling remained pure deuterium. The measurements show that the edge tritium concentration remained low, of the order of a few per cent, for these pulses. The final experiment was a pair of pulses at 4.2 MA/3.6 T (but the same configuration), with the same 10 MW of NBI, but in this case pure deuterium, whilst the gas and walls were tritium rich. Here the tritium concentration was measured to be 79%.

Table 1 shows the detailed edge measurements for these three experiments and a representative sample of the DD data. The table includes the alpha power (as measured by the DT neutron rate) and the edge fast particle pressure computed with the self-consistent code CHEAP (CHarge Exchange Analysis Package) [26], which is bench-marked by computations with the TRANSP code. The contribution from fast particles to the edge pressure is only about 10–20% of that from the thermal plasma but is computed to increase with beam T/(T+D) concentration.

Figure 3 shows the measured edge total thermal pressure, and electron pressure, at the giant ELM (which terminates the high performance phase), as a function of measured edge isotopic composition for the three experiments and the DD reference discharges. In order to allow for the higher plasma current in the third DT experiment, the data point has been shown as both measured and scaled with plasma current taken at the onset of the giant ELM (an assumption which is justified in section 3.3). The figure shows variations within the alpha heating and mixture experiments, and between these and the DD pulses, which are outside the experimental uncertainty and shot to shot variation (if we take the DD data spread as indicative of these factors). The pure deuterium beam into the DT plasma is also unexpectedly low, especially if we include the adjustment for the slightly higher plasma current. Note that we have excluded pulses with outer modes.

Variations are also visible in Fig. 3 in the electron pressure following the same general trends, which is reassuring. However, there is no fall-off in electron pressure at high tritium concentration in contrast to the total pressure data. In fact, in the two discharges at the highest tritium concentration, there is a sawtooth crash just before the ELM, and, whereas the electron temperature measurement resolves the edge response, the time response of the CX diagnostic ($\sim$100 ms) does not. It is possible, therefore, that the edge ion pressure for these two discharges is underestimated, and therefore the fall-off at high tritium concentration should be treated with caution.

A perusal of the data of Table 1 might suggest that the edge pressure is correlated with one or more of the following: alpha power, thermal ion temperature, fast ion pressure or fast particle tritium concentration. In the following paragraphs these correlations are examined in turn.

Note that the 100% tritium pulse from the mixture experiment and the peak of the alpha heating series have similar alpha powers, which would lead to a conjecture that the alphas play a role in the transport barrier possibly via heating. If the fall-off in edge pressure at high tritium concentration were substantiated, this would support such a conjecture. However the alpha simulation pulse described in Section 2.1, and the pure deuterium beams into DT plasmas provide counterexamples. Of course, if the plasma response to the alpha heating were reflected in the edge parameters, which it is, then one would expect to see this reflected in the limiting edge pressure if this were sensitive to edge ion temperature

Table 1. Parameters of interest for a series of low power heated hot ion H modes with different tritium mixes in the edge plasma and in the neutral beams: (a) deuterium only discharges at 3.8 MA/3.4 T with different recycling conditions, including the discharges with additional ICRH to simulate the alpha particle heating that would occur in DT plasmas; (b) discharges with deuterium background plasma and fast tritium sources from the neutral beams, again at 3.8 MA/3.4 T; (c) discharges performed at 3.8 MA/3.4 T with similar tritium mixes in both the edge plasma and the beams (alpha heating experiment); (d) pulse 43021 at 4.2 MA/3.6 T (but the same configuration) with pure deuterium beams whilst the gas and walls were tritium rich

Pulse No.	T/(D+T) (edge) (%)	T/(D+T) (beams) (%)	P_{NBI} (MW)	P_{ICRF} (MW)	P_α (MW)	$n_{e,edge}$ (10^{19} m^{-3})	$T_{e,edge}$ (keV)	$T_{i,edge}$ (keV)	$Z_{eff,edge}$	p_{edge} (kPa)	p_{fast} (kPa)
41069	0	0	6.0	0	0	3.07	4.53	5.22	2.20	42.99	7.06
44401	0	0	10.8	0	0	3.74	3.90	3.88	2.10	40.49	5.74
42578	0	0	10.6	0	0	3.75	3.90	3.90	1.86	42.75	5.23
41071	0	0	6.0	0	0	4.07	3.94	3.92	2.11	46.12	5.16
41067	0	0	10.6	0.87	0	3.06	4.81	5.31	2.31	43.28	7.96
41068	0	0	10.4	1.97	0	3.02	5.79	5.0	2.20	47.21	7.27
42647	4	25	10.9	0	0.58	3.92	3.92	3.83	2.17	42.03	7.72
42657	5	60	10.1	0	0.97	4.03	4.82	4.36	1.97	53.49	10.86
42656	5	100	8.3	0	0.91	3.98	4.87	4.05	1.72	53.32	8.50
42870	29	21	10.1	0	0.75	3.23	4.22	4.65	2.28	46.0	8.31
42856	63	45	10.5	0	1.40	3.60	5.81	5.21	2.39	58.59	8.62
42847	71	70	10.2	0	1.50	3.79	5.46	5.40	2.17	60.48	11.85
42840	84	100	10.6	0	0.77	3.63	5.50	5.33	2.55	55.54	12.88
43011	97	100	10.5	0	0.30	4.21	4.80	4.14	2.97	51.18	11.62
43021	79	0	10.4	0	1.06	3.32	5.24	4.68	2.60	50.68	6.56

for example (as discussed in the next paragraph). At this juncture, it should be recalled that the alpha heating data show, [2], a maximum in the confinement time at the maximum alpha power, similar to that seen in the pedestal pressure of Fig. 3 assuming the sawtooth effect on edge ion temperature is negligible (see above). This raises the intriguing possibilities that either the raised pedestal contributes to the core confinement improvement or the same mechanism changes both core confinement and pedestal. If this were the case, it is not clear why a similar mechanism does not apply to the alpha simulation pulse of Fig. 1 and the 100% tritium beam into deuterium plasma pulse. This is an active area of current investigation and will not be reported on further in this article.

There is indeed a peak in the edge ion pressure for the three pulses with high alpha power in the alpha heating series, which might suggest a correlation of limiting edge pressure with the thermal ion Larmor radius. However, the 60 and 100% tritium beams into pure tritium plasmas have a high edge pressure but not a high edge ion temperature. The pure deuterium beam into tritium rich plasma has

one of the larger thermal ion Larmor radii in the set but a low pedestal. An examination of a thermal orbit type model is made in Section 3 and compared with a wider data set, including full power beam only data where the edge ion temperature is largest.

There is a correlation of thermal edge pedestal pressure and the calculated fast ion pressure if the fall-off in pedestal pressure at high tritium concentration is assumed to be an artefact of the poor time resolution of the CX measurements. For this to be a satisfactory explanation of the data, the fast ion pressure would have to have a stabilizing effect on the ballooning stability. It is not at all clear why this should be so, but it could turn out to be a profitable area of theoretical research.

Finally, we turn attention to the last possibility mentioned in the list above, that the pedestal height is influenced by the fast beam injected species at the edge. In this respect, it is perhaps significant that the elevated pedestal pressure is found for high beam tritium concentration in both the alpha heating and mixture experiments, and a low pedestal is found for both the alpha simulation pulse and the injection of

pure deuterium beams into a DT plasma. In this case, it would be necessary to assume that the fall-off in pedestal at the highest plasma tritium concentration is an artefact (see the caveat above), or lies within measurement error. It is certainly a plausible hypothesis and is explored extensively in this article.

The low tritium beam concentration (21–25%) cases, in both the alpha heating and mixture experiments, have a pedestal height comparable to the pure deuterium beam cases. This might suggest that there is a threshold level of edge fast particle concentration before the fast particles affect the edge. It is expected that the orbit loss of fast particles would create a radial electric field [17] that is sufficient for turbulence suppression provided that the concentration exceeds a certain level (about 1% of the thermal density in our case).

On such an hypothesis, a difference in pedestal height would also be expected if the beam voltage is changed sufficiently. In fact it is systematically observed on JET that discharges employing the higher energy beams have longer ELM-free periods than those which employ the lower energy beams [27] and that higher pedestal pressures are observed in the former case. As an example, Fig. 4 shows some time traces of a pair of deuterium discharges at 3.8 MA/3.4 T and similar total beam power, ~10 MW. Discharge 42590 uses about 8 MW of 140 keV beams, whereas 42612 uses about 8 MW of 80 keV beams. In each case the remainder is made up of the other energy component. This example shows that the ELM-free period is longer with the larger high energy beam component and the electron pedestal pressure at the ELM is larger by 10%, which is only slightly larger than the measurement uncertainty of 8%. Clearly the effect is too small to be, by itself, a convincing demonstration, but serves to place an upper limit on the magnitude of any effect. The figure shows the slowing down averaged fast particle energy (at the edge), $\langle E_{fast} \rangle$, for the two cases as calculated by the CHEAP code. This differs by 20% between the two discharges, similar to the average injected particle energy, suggesting that any dependence upon fast ion energy scales at most like $\sqrt{\langle E_{fast} \rangle}$. In Section 3 such scaling ideas are developed further.

Additional evidence of the fast particle effects comes from the results obtained from the steady state ELMy H modes [28]. In particular, the influence of the fast particle component at the edge on the ELM behaviour is demonstrated in RF heated
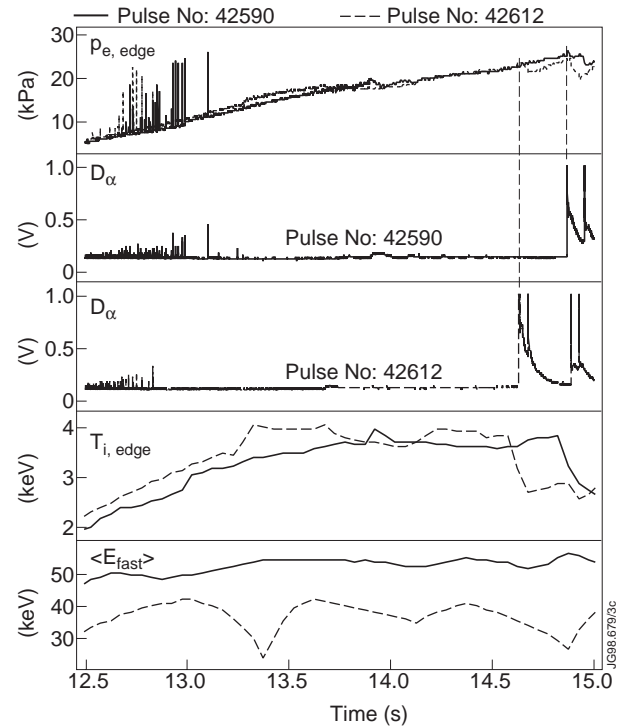

Figure 4. Time traces of two comparable pure deuterium discharges, pulses 42590 and 42612. Both discharges have similar NBI heating (~10 MW), but high energy beams dominate in pulse 42590.

discharges where the deposition profile of the fast particles was shifted to the edge by applying part of the heating power to the edge [28].

3. Edge transport barrier width

3.1. Models

Different models for the width of the edge transport barrier have been proposed since the discovery of the H mode. The oldest one, which is related to the turbulence stabilization by an externally imposed radial electric field [8], assumes that the width of the edge transport barrier, Δ_{bar}, is controlled by the ion orbit losses. This implies that the barrier width, Δ_{bar}, is proportional to $\sqrt{\varepsilon}\rho_{\theta i}$ with $\rho_{\theta i}$ being the poloidal ion Larmor radius. It was assumed in Ref. [7] that the transport barrier width is controlled by the losses of the thermal ions. However, it was found that Δ_{bar} should be a few (3 to 5) ion banana orbit radii in order to match the pressure at the top of the edge transport barrier with ballooning stability criteria [29].

Another idea, which was discussed recently, is that the transport barrier width is controlled by the radial correlation length of the turbulence itself [9–12]. This idea is actually twofold. Firstly, the radial correlation length is a reasonable measure for the turbulence suppression length by itself. Secondly, the radial correlation length is a good measure of the radial electric field width which is self-induced by a non-linear wave cascade. Three different expressions for the radial correlation length have been proposed: $\Delta_{cor} \approx \rho_i \propto \rho_{\theta i}$ [7], $\Delta_{cor} \approx \sqrt{\rho_i a}$ [10, 11] and $\Delta_{cor} \approx \sqrt[3]{\rho_i^2 a}$ [12].

The next concept is the idea of turbulence suppression by the finite ion Larmor radius [13–15]. We can expect this mechanism to be effective in suppressing the short wavelength turbulence with characteristic radial correlation length of the order of the ion Larmor radius.

It was also suggested that the width of the transport barrier could be controlled by the atomic physics processes such as the ionization of cold neutrals [16]. The physics behind this idea is that neutrals can act as an agent which takes the momentum from the ions and in this way control the shear in the plasma rotation. If this is the case, we might expect the width of the transport barrier to scale as: $\Delta_{bar} \approx \sqrt{V_{Ti}^2 / n_e^2 \langle \sigma v_e \rangle_{ion} \langle \sigma v \rangle_{cx}}$, where $n_e \langle \sigma v_e \rangle_{ion}$ is the rate of the cold neutral ionization and $n_e \langle \sigma v \rangle_{cx}$ is the rate of the charge exchange between neutrals and ions.

As we discussed earlier (Section 2.2), in some situations the width of the transport barrier could also be controlled by fast particles. In that case, the characteristic width of the barrier should be of the order of the banana width of the fast ions, i.e. $\Delta_{bar} \approx \sqrt{\varepsilon} \rho_{\theta i}^{fast}$. For a typical 3.8 MA/3.4 T hot ion plasma with a fast particle energy of ~70 keV, it gives $\Delta_{bar} \approx 0.63 [\langle E_{fast} \rangle \ (\text{keV})]^{1/2} \approx 5$ cm, which is consistent with the experimental measurements [30]. In the remainder of Section 3 we develop these ideas in such a way as to permit comparison with a wider data set.

3.2. Predictions for scaling of barrier height

The direct determination of the edge transport barrier width requires simultaneous detailed measurements of the electron density, electron temperature, ion temperature and Z_{eff} profiles. This has proven very difficult on JET due to the steep gradients at the edge and inadequate spatial resolution of the diagnostics for this purpose [30]. As an

alternative approach we adopt a simplified method [11] based on the assumption that the onset of the type I ELMs is controlled by the ballooning stability limit for the scaling of the edge barrier width, using the measurements at the top of the edge pedestal ($R = 3.75$ m, or $r/a \sim 0.9$).

Assuming that the giant (type I) ELMs are triggered by the edge ballooning instability, we can obtain the following expression for the critical pressure gradient [31]:

$$\nabla p^c \approx p_{edge}^c / \Delta_{bar} \propto B_\phi^2 / Rq^2 \varphi(s)$$

where p_{edge}^c is the critical pressure at the top of the barrier, B_ϕ is the toroidal magnetic field and q is the safety factor. $\varphi(s)$ depends on the magnetic shear and other details of the magnetic configuration within the barrier. With the same magnetic configuration, the following simple relation for the critical edge pressure is obtained:

$$p_{edge}^c \propto I_p^2 \Delta_{bar}$$

where I_p is plasma current.

If the width of the edge transport barrier is given by the poloidal Larmor radius of fast ions, i.e. $\Delta_{bar} \propto \sqrt{\langle M_{fast} \rangle \langle E_{fast} \rangle} I_p^{-1}$, we then obtain

$$p_{edge}^c \propto \sqrt{\langle M_{fast} \rangle \langle E_{fast} \rangle} I_p$$

where M_{fast} and E_{fast} represent averaged mass and energy, respectively, of fast particles.

Assuming the edge transport barrier is controlled by the poloidal Larmor radius of the thermal ions gives

$$p_{edge}^c \propto \sqrt{M_{eff} T_i} I_p$$

where M_{eff} is the effective mass of the DT isotopes at the edge.

These two models, together with other models discussed in Section 3.1, are compared with a wide range of JET hot ion ELM-free H mode data in Section 3.3.

3.3. Comparisons of data with model predictions

In this section the additional data to be included are introduced, a statistical analysis of the data is performed and finally the data are compared graphically with the models.

So far in this article we have considered only data from the low power experiments. Now some testable models have been proposed it is appropriate to consider a larger data set, in particular, so as to test

whether the trends already reported are manifested in the full power high fusion performance experiments in the hot ion ELM-free H mode. All eight such DT pulses as detailed in Ref. [1] are included together with their corresponding DD references. In addition, the following DD experiments are included: plasma current scans [25], performance optimization scans with both neutral beam only and combined neutral beam and ICRF [32], power step down experiments [27] and reference pulses for the comparison of the Mark I and Mark II divertors. A total of 80 pulses have been selected (including the 16 DT pulses) as representative of the regime. All these experiments use the same basic plasma geometry (elongation, $\kappa \sim 1.81$, and triangularity, $\delta \sim 0.36$). In particular, the separation between separatrix and outer limiter remains essentially constant, between 0.04 and 0.06 m, such that the reference measurement position (at 3.75 m) remains meaningful. The EFIT estimate of edge shear Sh_{95} has an average value of 3.6 and though there is some scatter in the estimate of this parameter (RMS variation ± 0.2) this appears to reflect only the measurement uncertainty and is not considered further in this analysis. In the data set the plasma current, I_p, varies from 1.6 to 4 MA, T_i (at $R = 3.75$ m) varies from 3 to 7 keV and T_i/T_e varies between 1 and 1.6 again at 3.75 m. These data are taken as close as possible to the giant ELM which terminates the high performance phase, and subsequent ELMs are ignored. In nine of the pulses selected an outer mode appears to clamp the edge parameters as described in Ref. [25] at values of pedestal pressure between 0.5 and 0.7 of the values observed in otherwise similar pulses. Such clear-cut examples are excluded from the analysis given hereafter, but some cases where the outer mode appears just before the ELM without appearing to affect the pedestal remain in the data set.

For each of the models a simple least squares fit (constrained through the origin) is applied, and the standard error and adjusted R^2 are computed. The standard error is computed from the mean square residual in the usual way and reflects the best estimate of the measurement error on the assumption that this is constant. Even if this assumption is not strictly true, we can nevertheless use this parameter as a quantitative description of the scatter between model and data. The parameter R^2 describes the portion of the total variation ascribed to the model adjusted for the degrees of freedom for error. A low value of R^2 means the model is a poor description of the data (or that there is an insufficient number of

data points) and 1 indicates a perfect fit. In such an analysis the estimate of the independent variable is assumed to have zero error, which for our case means that we have neglected the effect of the error in T_i on the independent variable.

In all, four models for the pedestal height are tested based on the discussion of Sections 3.1 and 3.2, together with a simple scaling with I_p alone. It is not clear, for the fast particle model, how the fast particles should be weighted and therefore three variants of this model are taken, a simple slowing down average over all energy components and species (injected from both octant 4 and octant 8 beams) as in Ref. [11], an average over all injected species and, finally, the species with the largest Larmor radius (i.e. the full energy component of the higher voltage injector). The results from these seven tests are listed in Table 2, ordered by the value of R^2.

The first striking conclusion is that, on this analysis, none of the models can be rejected out of hand as being an unacceptable description of the data but that four of the tests show somewhat worse agreement with the data than the scaling with I_p alone. In particular, the standard errors are not inconsistent with the estimate of measurement error derived from the individual measurements, which is estimated as ± 5 kPa at 50 kPa. This provides encouraging support for the quality of the measurements, and indicates a good degree of shot to shot reproducibility. However, it is not encouraging from the point of view of separating out the underlying physics. It is worth noting, at this stage, that there is a trend for the fast ion pressure to be higher with tritium rich beams, and the fast ion pressure can reach $\sim 20\%$. However, including the calculated fast ion pressure and performing the same analysis with total pressure makes essentially no difference to the standard error or R^2.

For the two models with a stronger than linear dependence on I_p, this statistical approach indicates that these would be 'reasonable' descriptions of the data if the error were constant throughout the data. In particular, if the error at $I_p = 1.6$ MA were ± 7 kPa for a measured value of pedestal of 20 and 24 kPa at this current, this would be consistent with the predicted pedestals of about 14 kPa. However, the estimated measurement error in this case is ± 3 kPa, so the discrepancy is 3 times the measurement error, and this is sufficient to exclude these models. They are not considered further in this article. All the remaining models have a linear scaling of pedestal height with I_p and this justifies the proposed normalization of the pure deuterium beam

Table 2. Statistics of the least squares fit for the different models for the pedestal height, as discussed in Sections 3.1 and 3.2. In particular, the fast particle model includes three variants, corresponding to the different weightings of the fast particles: a slowing down average over all energy components ($\langle E_{fast} \rangle$) and species ($\langle M_{fast} \rangle$), an average over all injected species ($\langle M_{inj} \rangle$), ($\langle E_{inj} \rangle$) from both octant 4 (80 kV) and octant 8 (140 kV for deuterium, 188 kV for tritium) beam boxes, and, finally, the species with the largest Larmor radius (i.e. the full energy component of the higher voltage injector)

Dependent variable	Independent variable	Slope	Adjusted R^2	Standard error (kPa)
p_{edge} (th)	$I_p(\langle M_{fast} \rangle \langle E_{fast} \rangle)^{1/2}$	1.26	0.863	7.77
p_{edge} (th)	$I_p(\langle M_{th} \rangle T_i)^{1/2}$	4.15	0.867	7.64
p_{edge} (th)	$I_p^{4/3}(\langle M_{th} \rangle T_i)^{1/3}$	4.082	0.875	7.36
p_{edge} (th)	$I_p^{3/2}(\langle M_{th} \rangle T_i)^{1/4}$	4.044	0.876	7.35
p_{edge} (th)	I_p	13.85	0.893	6.75
p_{edge} (th)	$I_p(\langle M_{inj} \rangle \langle E_{inj} \rangle)^{1/2}$	1.06	0.912	6.03
p_{edge} (th)	$I_p[\mathrm{Max}(ME)]^{1/2}$	0.763	0.927	5.40

to the DT discharge in Fig. 3, as described earlier. Indeed, with such a normalization, 10 out of the 16 DT pulses have pedestals higher, by up to 25%, than the maximum pedestal observed in pure deuterium. Clearly there is an effect to be explained.

As regards the remaining models we simply note that thermal and average fast particle models provide comparable, and not unsatisfactory, qualities of fit, but that this quality of fit improves as the fast particles are weighted towards the components with larger Larmor radii. It is now time to compare the data in more detail with some of these models.

Figure 5 shows the measured thermal pedestal height plotted against the predictions of the thermal model. The figure shows a line for the fit of Table 2 expressed as a multiplier of the thermal poloidal banana width, which confirms the direct measurement mentioned earlier, that the width is systematically ∼5 times the gyroradius. The plasma current scans are well described by the model, confirming the plasma current dependence. Interestingly the alpha heating series follows the expected behaviour, i.e. pedestal increasing with T_i, but the mixture experiment shows a varying pedestal at the same T_i. The pedestal height in the high power neutral beam only deuterium data appears comparable to the low power data despite a large change in T_i. Note that the highest pedestal in the deuterium data is about 53 kPa, and many of the DT data lie above this. Indeed if we consider high power data, there is a large spread in pedestal values (from 40 to 67 kPa) for similar values of $\rho_{\theta i}^{th}$. This spread is more than twice the measurement error. If the model were valid, this would indicate that other sources of error or variation are

affecting the data. It is hard to exclude such a possibility, and therefore we cannot reject the model. This conclusion is consistent with the statistical analysis presented earlier. However, the source of error or variation needs to account for the observed changes in pedestal height between DD and DT.

Figure 6 shows the measured thermal pedestal height plotted against the predictions of the fast particle model, using the same weighting as in Ref. [11], where the averaging is performed over the slowing down of fast ions from both injector boxes (at octants 4 and 8). The figure shows a line for the fit of Table 2 expressed as a multiplier of the average fast ion poloidal banana width. This model describes well the I_p variation in the DD data and groups the high current data (low power, high power neutral beam only and neutral beam RF) as a 'blob' with a small vertical scatter comparable to the estimated measurement error. The model ascribes the small variation in pedestal height between low power and high power (mentioned earlier in Section 2) to differences in I_p that arise when a current rampdown is employed [25], because the ELM limit is reached more quickly at high power. There is a single outlier in the deuterium data (the same discharge stands out in Fig. 5). A closer examination reveals no reason that this should be treated as a special case, and the pulse has been left in the data set to receive due statistical weight. In this presentation of the data, the low beam tritium concentration pulses from the alpha heating and mixture experiments group with the low power DD data since the average energy is dominated by the deuterium beams. The DT data with near optimal beam and
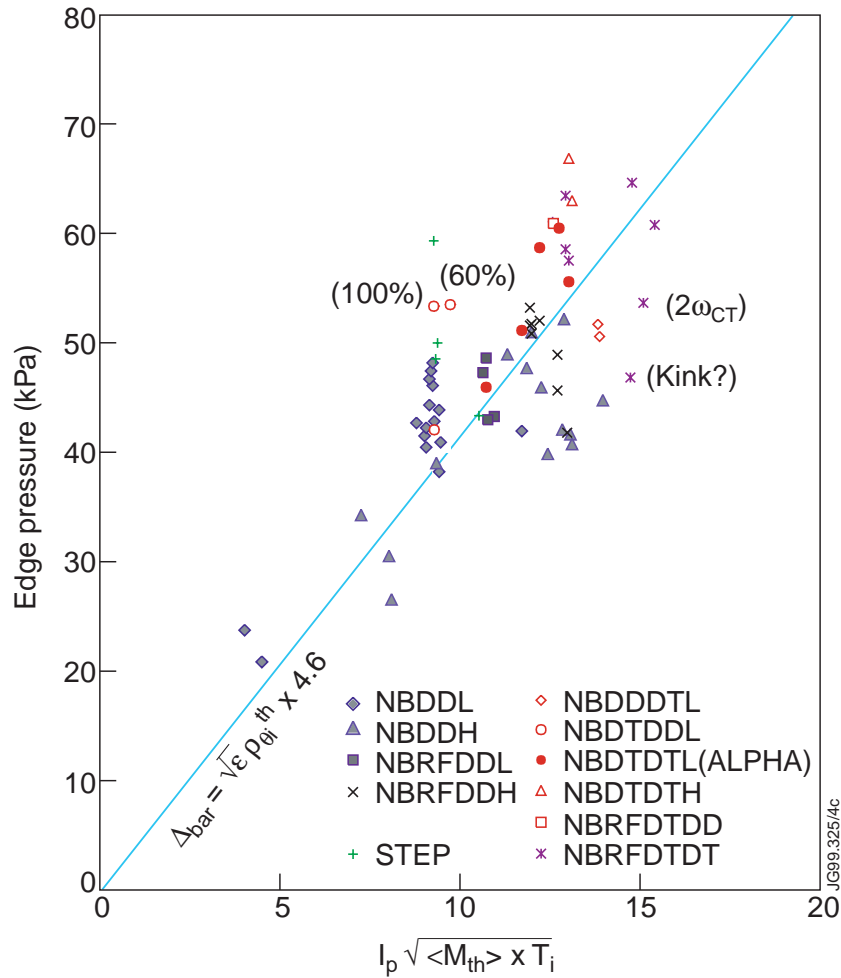
Figure 5. Scaling of the edge transport barrier width with the Larmor radius of the thermal ions for DD and DT ELM-free hot ion H modes including the following discharges: deuterium only with low power ($\sim$10 MW) NBI heating (NBDDL); deuterium only with high power NBI heating (NBDDH); deuterium only with combined low power NBI and ICRF heating (NBRFDDL); deuterium only with combined high power NBI and ICRF heating (NBRFDDH); power step-down experiment (STEP); mixture experiment (NBDTDDL); DT discharges with lower power pure deuterium beam (NBDDDTL); alpha heating experiment (NBDTDTL); DT discharges with high power DT beams (NBDTDTH); deuterium only discharges with combined DT NBI and ICRF heating (NBRFDTDD); DT discharges with combined DT NBI and ICRF heating (NBRFDTDT). In addition, the best fit corresponds to the edge pressure values expected from the ballooning instability limit if the barrier width is 4.6 times the Larmor radius of the thermal ions, as indicated in the figure. I_p is in megamps and T_i in kiloelectronvolts.

plasma mixes (low power, high power neutral beam and neutral beam RF) stand out clearly in this presentation as having a significantly higher pedestal than their DD counterparts. The magnitude of the change in pedestal height is in accord with the predictions for this model. However, the three low power tritium rich discharges have a pedestal which is intermediate between the pure DD and optimal DT (as
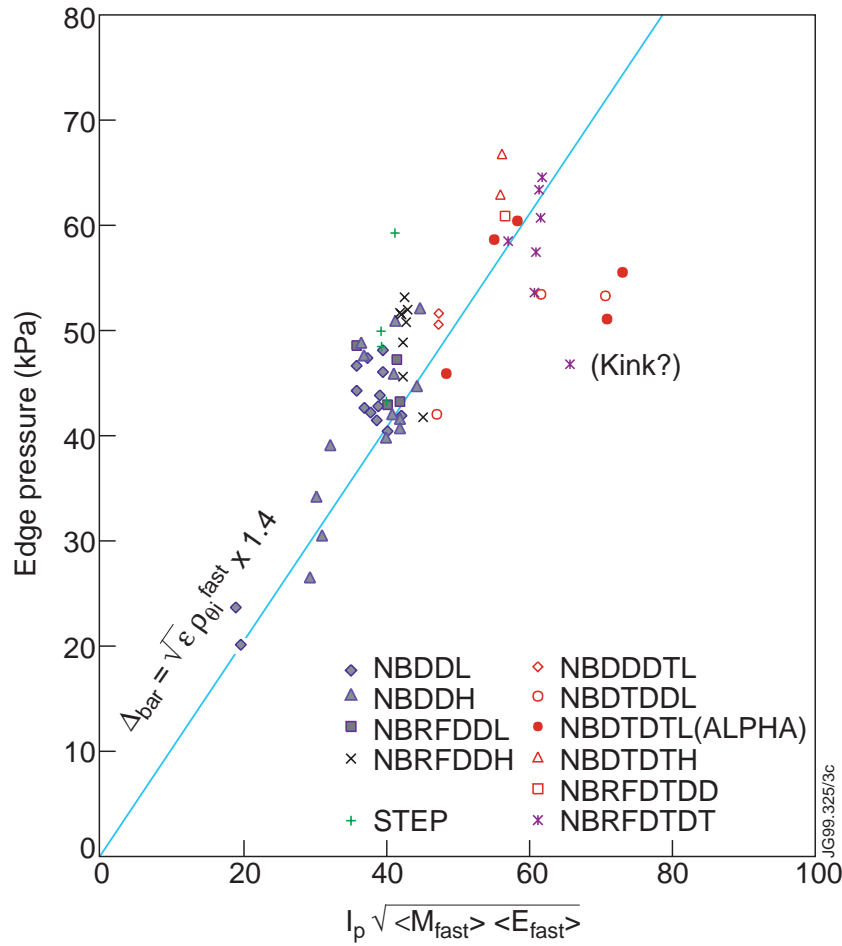
Figure 6. Scaling of the edge transport barrier width with the Larmor radius of the fast particles for DD and DT ELM-free hot ion H modes with a simple slowing down average over all energy components and species of the fast ions. The solid line indicates the best fit as well as the predicted values if the barrier width is 1.4 times the Larmor radius of the fast particles. I_p is in megamps and E_{fast} in kiloelectronvolts.

already shown in Fig. 3), whereas the model predicts these discharges should have the highest pedestal. They manifestly do not! Two of the discharges have a sawtooth just before the ELM which might cause the ion pedestal to be underestimated, as mentioned in Section 2.2, but it seems unlikely that this could account completely for the discrepancy between measurement and prediction. The remaining outlier in the DT data has an outer mode 100 ms before the ELM, which is a much shorter duration than the cases excluded, and it is not clear whether the pedestal is clamped. These three tritium rich pulses and the DT outlier contribute half the mean square residual of the fit. Without them the adjusted R^2

increases from 0.863 to 0.934, which indeed would make an excellent fit. Further experiments in DT would be required to clarify whether these pulses are typical or not and, until then, this model cannot be described as superior to the thermal model.

The statistical analysis identified the best fit to the data set with a fast ion model set by the largest Larmor radius. For our data set this is the full energy component of the higher energy injector box. There are no pulses in the data set without at least some power from the high energy box, since this is required for the charge exchange measurements. Figure 7 shows the data plotted against this scaling, with the line for the best fit expressed as a multiplier of the
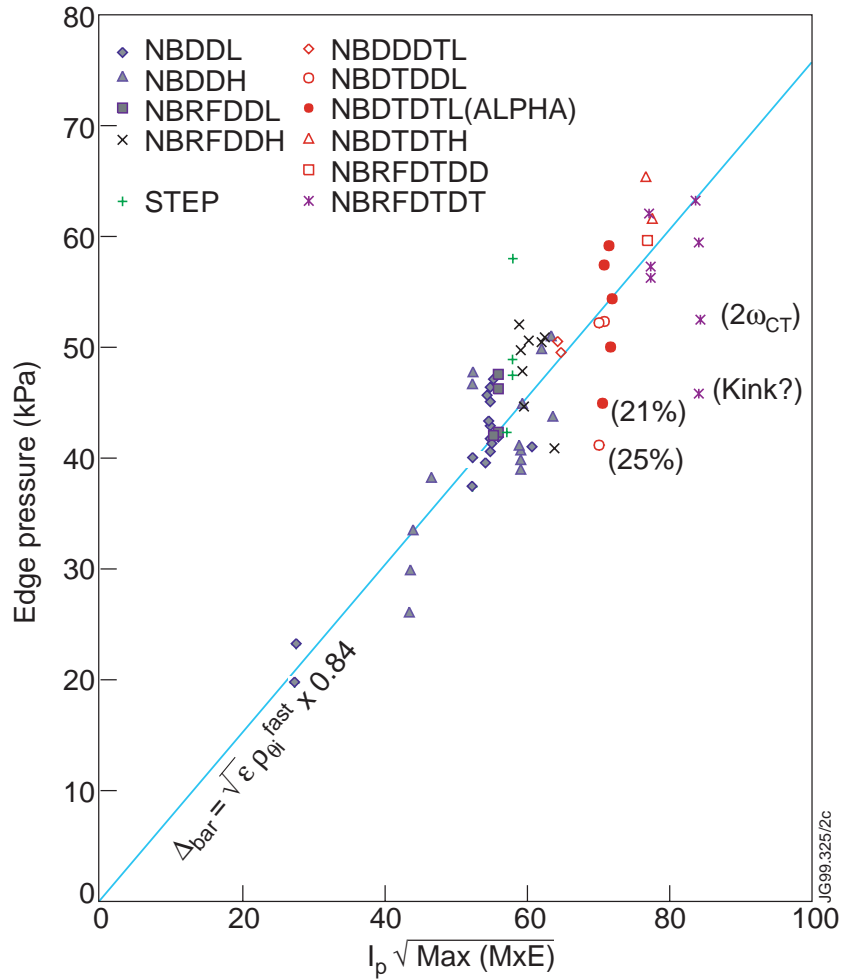
Figure 7. Scaling of the edge transport barrier width with the Larmor radius of the largest Larmor radius of fast ions. The best fit corresponds to the edge pressure values expected from the ballooning instability limit with $\Delta_{bar} = 0.84\sqrt{\varepsilon}\rho_{\theta i}^{fast}$.

poloidal banana width of fast particles. In both fast ion models the measured pedestal height is consistent with the fast ion orbit size given the uncertainties in calculating the ballooning limit. Given that $\sqrt{(ME)}$ is essentially constant for the deuterium data for both fast ion models, it is not surprising to find the deuterium data in Fig. 7 well described by the model, as discussed already for Fig. 6. In tritium an higher injection voltage was employed (150–155 kV as opposed to 135–142 kV in deuterium) and as a result $\sqrt{(ME)}$ is increased by about 30% in tritium over deuterium. The vertical banding of the DT data reflects variations in I_p. It can be seen that the bulk of the DT data also lie on the model prediction to within the estimated measurement error. Indeed the

standard error of Table 2 supports this and suggests that the four outliers in the DT data are not very significant. There are two high power DT outliers one of which is the same outer mode discharge described in the previous paragraph. The other is the only pulse where the RF employed some $2\omega_{cT}$ heating in addition to the usual ω_{cH} [1], and of course there is no pure deuterium reference for this. The other two outliers are the 21–25% tritium beam cases from the alpha heating and mixture experiments described in the discussion of Fig. 3. In these two discharges the tritium fast ion density is about 0.4%, compared with a total fast ion density of about 1.2%. The tritium fast ion density in the other low power shots with tritium beams is about 1% or greater. It could well

be the case that these discharges are consistent with the suggestion [17] that there is a critical fast ion density (of the order of 1%) in order for the fast particles to be effective in stabilizing turbulence. If it is assumed that the dominant fast particles in these two discharges is deuterium then these two points return to good agreement with the model. The two discharges with pure deuterium beams into DT have a low pedestal as expected from the model. To summarize, this model is the most attractive description of the data.

3.4.   Discussion

From the analysis of the complete hot ion ELM-free H mode edge database presented in this section, the following conclusions can be drawn. Firstly, there is a small but noticeable 'isotope' effect in the high power data of similar magnitude to that illustrated for the low power data in Section 2. Secondly, the thermal ion model for the pedestal height cannot be unambiguously excluded, but the variation in the data is larger than expected. The discrepancy in the implied barrier width also remains puzzling. Thirdly, the fast ion model brings the implied barrier width in line with the magnitude of the fast ion banana width. Finally, the fast ion type of model describes much of the data well, but it is necessary to either (a) exclude the high tritium concentration discharges or (b) weight the model to the higher energy part of the fast ion distribution.

At this point it may be useful to make some comparison with the data for ELMy H modes, without gas fuelling [11], and the data for ELMy H modes with strong gas fuelling [33] in JET. In the former reference it was concluded (albeit on the basis of 12 pulses) that the slowing down averaged fast ion model gave a superior fit to the data, whereas in the latter (with a much larger set of discharges) the thermal model was preferred. In contrast to the data presented in this article, both these references deal with higher edge density where T_i and T_e are equal, so it is possible that the three regimes are just different. It is also possible that the thermal model applies to all three cases.

Reference [33] discusses the fast ion density, which is shown to lie in the range 0.2–1.5%. In our data, the total fast ion density is in the range 1–3.5%. Reference [11] does not quote fast ion densities, but for the 95% deuterium and 95% tritium discharges of Figs 5 and 13 of that reference the fast ion densities are 1.1 and 1.2%, respectively. It is plausible

therefore that for fast ion densities that are less than the order of 1% fast ions are not important and that for fast ion densities that are larger than the order of 1% fast ions play a role, thus explaining the differences in the conclusions of these articles. It is possible the differences between our data (which are thoroughly exposed in this article) and the more limited presentation of reference Ref. [11] arise from changes to the slowing down distribution which are not well represented by the ad hoc formulations proposed.

It should be apparent, therefore, that a definitive demonstration of the possible effects of fast ions on the transport barrier remains to be devised. The experimental data on pedestal height are unlikely to provide such a demonstration and, in particular, more direct measurements of the barrier region seem to be required. However, in the meantime, and in the remainder of this article, the implications of a fast ion dominated transport barrier are explored in terms of the losses through the barrier.

4.   Loss power through the transport barrier

4.1.   Neoclassical losses

Two main mechanisms of heat loss from the barrier region have been identified in hot ion H modes. The first one is related to the diffusive losses through the transport barrier and the separatrix. The second one is attributed to the non-diffusive losses of the hot ions via their charge exchange with the cold neutrals and subsequent escape from the confinement zone.

The diffusive losses are caused by the finite ion and electron thermal conductivity within the transport barrier, which in the best cases could be reduced to neoclassical level [5]. With the assumption that anomalous ion transport within the transport barrier is completely suppressed in the hot ion H mode, we then obtain the following expression for the ion heat flux [6, 7]:

$$q_i \approx -n_i \chi_i^{neocl} \nabla T_i. \tag{1}$$

Since the edge transport barrier is quite narrow $(\Delta_{bar}/a \ll 1)$, we can make the following substitution: $n_i \nabla T_i \approx -(n_i T_i)_{edge}/\Delta_{bar}$, which gives instead of Eq. (1),

$$q_i \approx (n_i \chi_i^{neocl} T_i)_{edge}/\Delta_{bar}. \tag{2}$$

It was assumed [8] that close to the separatrix (within the distance of the ion poloidal Larmor radius), the ion conductive neoclassical heat flux

is converted into the convective flux produced by the direct ion losses. To ensure plasma ambipolarity we could assume that either the electron anomalous transport is reduced to the level of the ion neoclassical transport, i.e. $\chi_i \approx \chi_e \approx D \approx \chi_i^{neo}$ [6, 7, 29], or that the direct ion losses are compensated by the influx of cold ions from outside the separatrix [8]. In the latter case the losses through the electron channel should be significantly reduced with respect to the corresponding losses through the ion channel ($q_e \ll q_i$). Due to limited experimental information, we cannot discriminate between these two cases at present.

For the non-diffusive channel of the energy losses, charge exchange between hot ions and cold neutrals, we can estimate the maximum charge exchange heat flux assuming 100% recycling from the wall. In this case the influx of cold neutrals should be equal to the outgoing flux of the ions. With the neoclassical transport barrier, the following expression for the particle flux through the separatrix can be obtained:

$$\Gamma \propto q_i/T_{i,edge} \approx (n_i\chi_i^{neocl})_{edge}/\Delta_{bar} \qquad (3)$$

where $T_{i,edge}$ is the ion temperature at the top of the transport barrier. To find the characteristic heat flux produced by the charge exchange losses we should multiply Eq. (3) by the characteristic ion temperature within the region of the most intensive charge exchange interaction. The numerical analysis [6] shows that this region is localized inside the transport barrier. Therefore, the charge exchange losses are qualitatively similar to the neoclassical losses through the transport barrier ($q_{cx} \sim q_i$) but could have a slightly larger magnitude.

It follows from the above analysis that the total heat flux through the separatrix (including conduction, convection, and charge exchange losses) is $P_{loss}^{ccx} \approx q_i + q_e + q_{cx} \propto q_i$, which is given by Eq. (2). Assuming that Δ_{bar} is controlled by the Larmor radius of the fast ions, we obtain the following expression for the loss power:

$$P_{loss}^{ccx} \propto n_{edge}^2 Z_{eff,edge} I_p^{-1} \sqrt{T_i/\langle E_{fast}\rangle}$$

provided that the fast ions have the same isotopic composition as the thermal plasma ions. $\langle E_{fast}\rangle$ is the average energy of fast particles including both deuterium and tritium fast ions. n_{edge} and $Z_{eff,edge}$ are, respectively, the density and Z_{eff} at the edge. Alternatively, with the assumption that Δ_{bar} is controlled by the Larmor radius of the thermal ions, we then obtain:

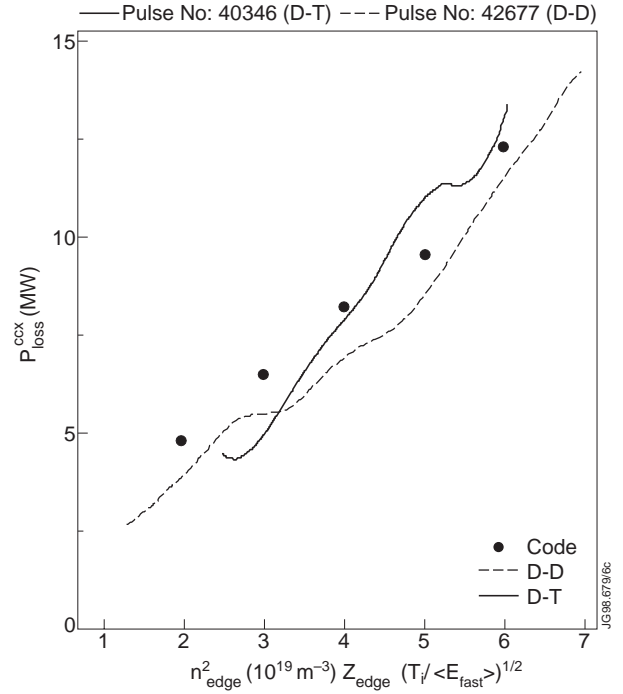$$P_{loss}^{ccx} \propto n_{edge}^2 Z_{eff,edge} I_p^{-1}.$$

Figure 8. Loss power from the DT (pulse 40346) and DD (pulse 42677) discharges against the predictions from the neoclassical models assuming the edge transport barrier width is proportional to the Larmor radius of the fast particles, together with the predictions from the JETTO code.

4.2. Loss power in DD and DT

The power loss through the separatrix is determined by subtracting the radiation inside the separatrix, $P_{rad,core}$, and the change in the content of thermal energy, dW_{th}/dt, from the total heating power absorbed by the thermal plasma, P_{in}^{th}, i.e.

$$P_{loss}^{ccx} = P_{in}^{th} - dW_{th}/dt - P_{rad,core}$$

where P_{in}^{th} is computed by TRANSP, including ohmic heating, the total thermal heating from the ICRF and the neutral beams (taking account of orbit losses, beam shinethrough and charge exchange losses), as well as the heating of the thermal plasma by rotation friction. In addition, the heating from the alpha particles is included for the DT discharges. W_{th} is also obtained from TRANSP analysis. $P_{rad,core}$ is measured by the bolometers.

Figure 8 plots the loss power, P_{loss}^{ccx}, against the predictions from the neoclassical models for two of the best fusion performance hot ion H modes, i.e. pulses 40346 and 42677, in the Mark II divertor with the neutral beam heating only and $I_p = 3.8$ MA, $B_T = 3.4$ T. Pulse 40346 is in pure DD with $\sim$19 MW

of neutral beam heating, while the DT discharge ($\sim$50%–50% D–T) has a higher fast particle energy from the tritium beams, and hence has higher neutral beam heating power ($\sim$23 MW) with a larger population in the high energy beam box. The experimental data are taken from the ELM-free period in the discharges. It appears that there is a rather good correlation between P_{loss}^{ccx} and $n_{edge}^2 Z_{eff,edge} \sqrt{T_i / \langle E_{fast} \rangle}$ as predicted by the neoclassical model based on the assumption that the transport barrier width is proportional to the Larmor radius of fast ions. It is to be mentioned that the ratio of $T_i / \langle E_{fast} \rangle$ is relatively constant for a given pulse during the ELM-free phase (see Fig. 4, for example). A plot of P_{loss}^{ccx} versus $n_{edge}^2 Z_{eff,edge}$ produces similar trends. In addition, Fig. 8 shows the loss power calculated by the fully predictive JETTO code [6] for the DT pulse, including the neoclassical and charge exchange losses, for comparison with the experimental scaling. As can be seen, the code predicts not only the dependence of the power losses on the edge plasma parameters but also gives quantitative agreement with the experimental results. For this case, the charge exchange loss is about the same as the neoclassical losses.

Since DT discharges appear to have a larger edge transport barrier width than that in DD discharges, we might expect that the energy content of DT plasmas should rise faster because of the smaller neoclassical and charge exchange losses. Combining this with the better ballooning stability at the edge, we might therefore expect higher performance in a DT plasma than in its DD counterpart. In fact similar levels of performances are delivered in the DD and DT hot ion modes. The detailed analysis of this surprising result must involve the core transport and lies outside the scope of this particle. Here we limit ourselves with some qualitative assessments. One possible explanation is as follows. If the core transport were controlled by a combination of a gyro-Bohm ($\chi_{gyro\text{-}Bohm} \propto \sqrt{m_i}$) and a Bohm type ($\chi_{Bohm} \propto m_i^0$) of turbulence as was proposed in the JET model [6, 7], then the transport in the central part of the plasma would be dominated by the $\chi_{gyro\text{-}Bohm}$, which is stronger in the DT mixture, offsetting the pedestal effect. This would thus degrade the core confinement. In addition, it is observed in the experiments that, in general, the edge density rises faster in DT, which could therefore result in a faster increase in the edge losses. Apart from the core confinement degradation, the possible difference in the edge recycling between the deuterium and tritium neutrals could also be responsible for the higher edge
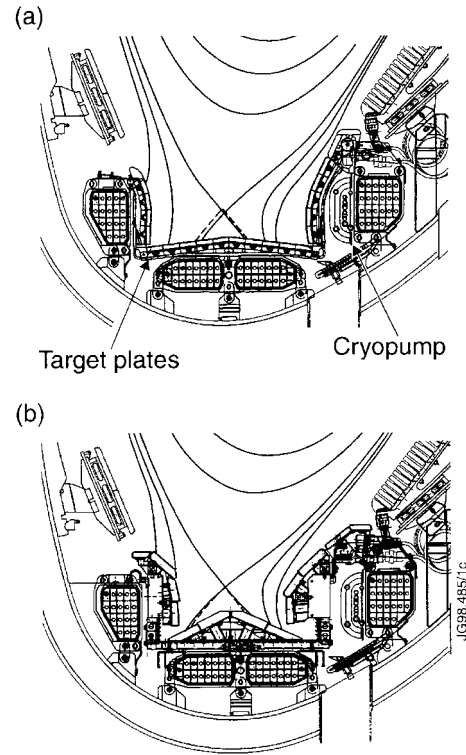

Figure 9. Poloidal cross-sections of (a) the JET Mark I divertor and (b) the JET Mark II divertor.

density in DT. In particular, the cold neutrals which are always present in the edge are much more localized near the separatrix in the case of a tritium plasma than a deuterium plasma, which might therefore lead to a relative increase in the edge plasma density in the tritium enriched plasma. In addition, the tritium beams can produce broader power and particle deposition profiles than the deuterium neutral beams, but the TRANSP analysis shows that the differences are actually very small.

5. Comparison between Mark I and Mark II divertors

5.1. Impurity behaviour

The Mark II divertor was designed with a more closed geometry compared with its Mark I predecessor, as shown in Fig. 9, to reduce the flow of neutrals back to the confined plasma. It was thereby hoped to reduce the loss power by charge exchange in the edge plasma and to reduce the impurity production by the neutrals in the main chamber, hence increasing the fusion performance. However, one unexpected result of the Mark II operation is that the impurity
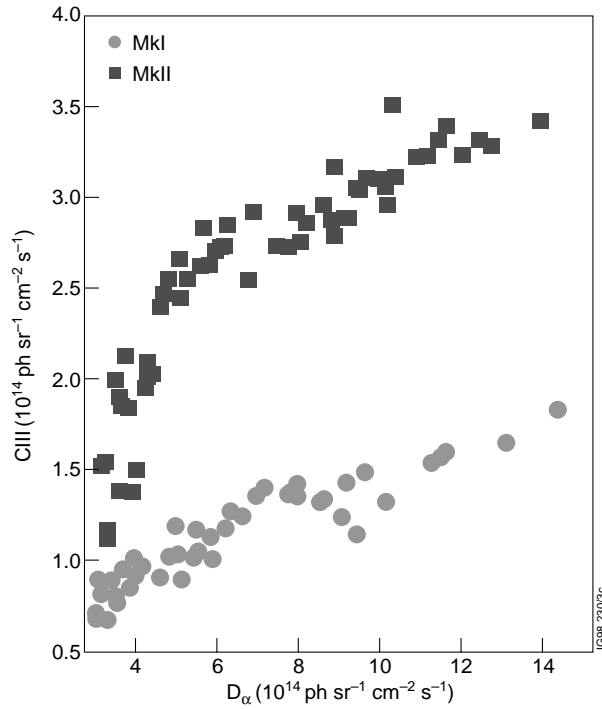
Figure 10. CIII photon emission from the outer divertor as a function of the D_α photon fluxes.

Figure 11. Comparison of $Z_{eff,edge}$ between the Mark I and Mark II results.

production yield at the divertor target is increased in Mark II relative to that in Mark I. The divertor impurity sources in the Mark I and Mark II divertors, are compared in Fig. 10, where the average CIII photon flux is plotted against the D_α intensity from the outer strike zones for the hot ion H modes during the ELM-free phase. As can be seen, the CIII intensity is about a factor of 2 higher in the Mark II divertor than in the Mark I divertor for a given D_α flux. The CIII and D_α emissions from the inner divertor show similar results. It is to be noted that the electron temperature and density at the target plate are very similar for Mark I and Mark II hot ion discharges at the strike points, as measured by the target Langmuir probes. Therefore, the higher CIII/D_α ratio suggests an increased impurity production yield at the Mark II divertor target. The best explanation for the higher yield is that the chemical sputtering yield is increased due to the higher base temperature of the Mark II divertor target plate [34]. Specific experiments with lower wall temperature in Mark II support this explanation [35].

The impurity concentration within the edge transport barrier inside the separatrix is determined by the impurity sources and the transport of the impurities through the SOL. Contrary to the high
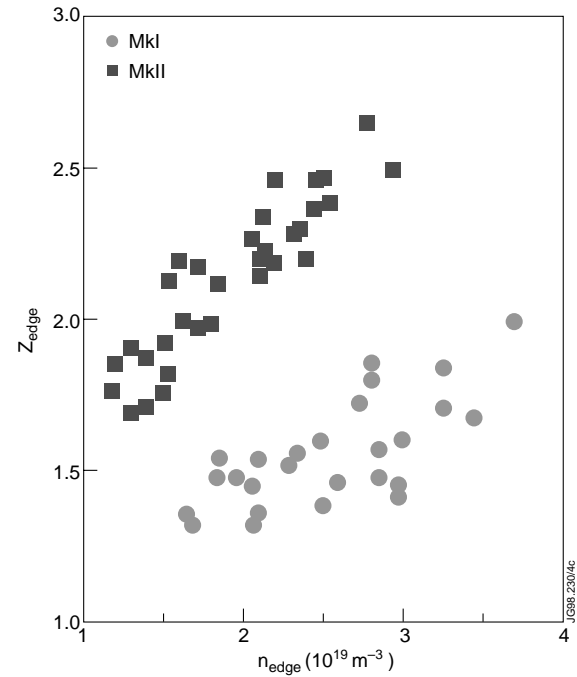
recycling regime [36, 37], the divertor/SOL screening for the impurities is poor in the low recycling hot ion regime [34]. Consequently, the higher impurity flux produced in the Mark II divertor results in a significant increase in Z_{eff} at the edge, upstream from the target, compared to Mark I, as illustrated in Fig. 11, where the measured Z_{eff} at the edge is plotted against the density at the edge for the pulses of Fig. 10. Analysis of the highest performance discharges with the EDGE2D/NIMBUS [38] codes shows [34] the higher Z_{eff} at the edge observed in the Mark II divertor, compared with that in Mark I, taking into account the change in the chemical sputtering yield with the different base temperatures of the Mark I (40°C) and Mark II (270°C) divertors.

Neoclassical transport implies that the power losses through the separatrix are explicitly dependent on the Z_{eff} at the edge. Indeed, a systematic increase in the power losses has been observed between Mark I and Mark II hot ion H modes. In particular, Fig. 12(a) compares the loss power and $Z_{eff,edge}$ for pulse 40346 (Mark II) with those for the Mark I DD hot ion H mode, pulse 33643. Pulse 33643 delivered the highest fusion performance in the Mark I campaign with similar NB heating power compared with the Mark II pulse. In addition, both discharges have the same plasma current and
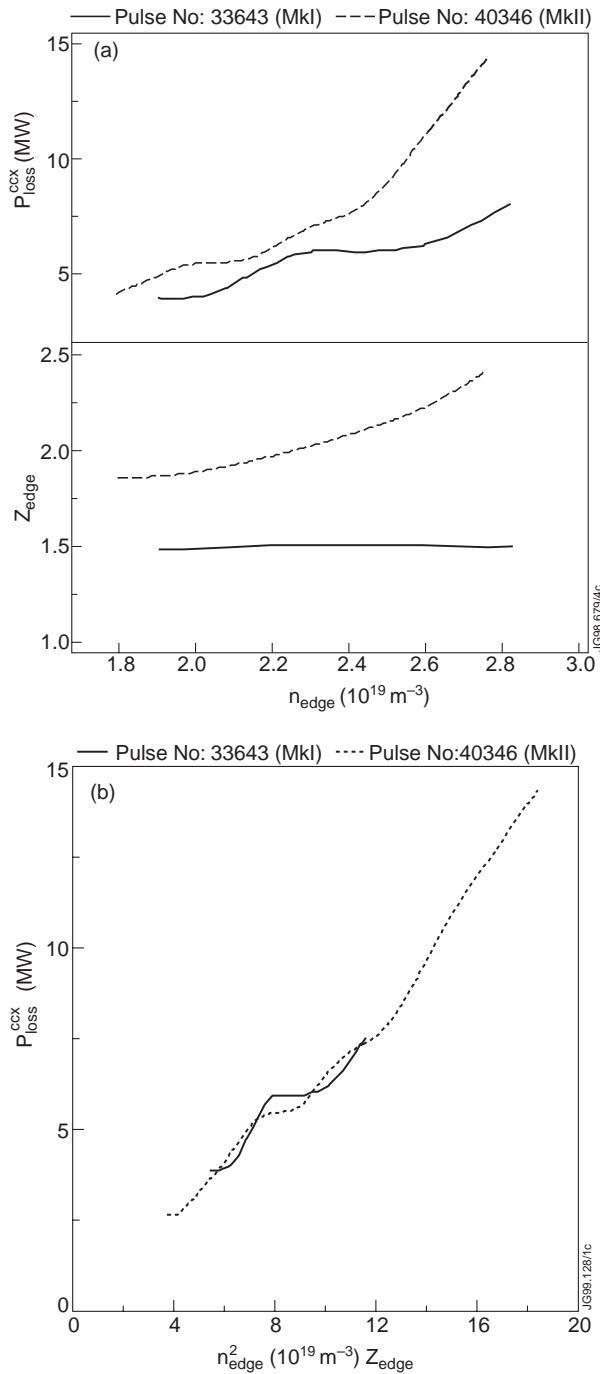
Figure 12. (a) Comparison of loss power and Z_{eff} at the edge between pulse 40346 (Mark II) and pulse 33643 (Mark I), which have the same plasma current and magnetic field (3.8 MA/3.4 T) and similar NBI heating ($\sim$20 MW). (b) Loss power versus $n^2_{edge}Z_{eff,edge}$ for the two pulses.

magnetic field (3.8 MA/3.4 T). As can be seen, the loss power in the Mark II hot ion mode is significantly higher, at a given edge density, than that in

the Mark I pulse, and correlates with a higher Z_{eff} at the edge.

In Fig. 12(b) the loss power is plotted against $n^2_{edge}Z_{eff,edge}$ for pulses 40346 and 33643. It appears that there is a good agreement with the neoclassical prediction. This agreement is made more convincing by the fact that loss power and edge Z_{eff} are significantly higher for the Mark II discharge, pulse 40346, at a given edge density, as shown in Fig. 12(a).

5.2. Effect of edge recycling

The rate of rise of the edge density is dependent on the recycling of neutrals from the main chamber and the divertor, in addition to the particle transport from the confined plasma core. It has been demonstrated in Ref. [3] that for hot ion H modes with the Mark I divertor, the minimum recycling condition is essential for maximizing the ELM-free period and improving the fusion performance. However, in going from Mark I to the more closed Mark II divertor the pressure of neutrals in the divertor increased by a factor of 2 and hence increase pumping. This strong divertor pumping has reduced the need for extensive conditioning for access to the hot ion regime and increased the reproducibility of the performance achieved [4]. However, the plasma density rise during the ELM-free phase is reduced, as shown in Fig. 13, where the divertor neutral pressure and the edge density are compared between the discharges in Mark I (pulse 33643) and Mark II (pulse 38093) with similar neutral beam particle source and gas fuelling. Consequently, additional gas fuelling has to be used to raise the central plasma density and reduce the beam shinethrough losses. In addition, it was found that the gas puff/bleed could reduce the Z_{eff}, and delay the core MHD in some discharges [24]. However, inevitably, the gas fuelling also increases the edge density [30].

Apart from the higher Z_{eff} at the edge, as described in Section 5.1, the higher edge density might also be responsible for the higher loss power observed in Mark II. To illustrate this, we have selected the data close to the peak performance from the best of Mark I and Mark II neutral beam and ICRF heated discharges, including both DD and DT hot ion H modes analysed by TRANSP. Figure 14 plots the loss power, P^{ccx}_{loss}, computed by TRANSP as a function of the edge density. As can be seen, the loss power is clearly higher in Mark II and is correlated with a higher edge density, except for pulse 38093 which has a lower edge density than that of the
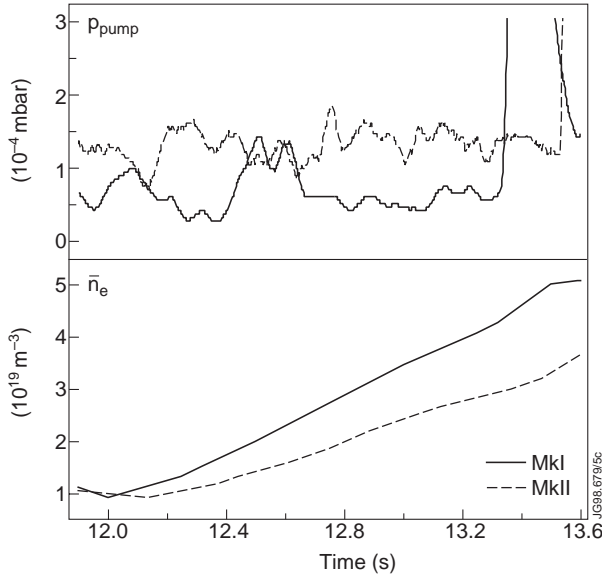
Figure 13. Comparison of the neutral pressure in the subdivertor (and thus pumping speeds) and the density evolution for two ELM-free hot ion H modes in the Mark I (pulse 33643) and Mark II (pulse 38093) divertors. The two discharges have similar NBI particle sources and gas fuelling.

Mark I discharge (pulse 33643). Note that at similar edge densities, the loss power is also higher in Mark II due to the higher Z_{eff}. A plot of P_{loss}^{ccx} against $n_{edge}^2 Z_{eff,edge} I_p^{-1} \sqrt{T_i/\langle E_{fast}\rangle}$ brings both the Mark I and Mark II data together and shows a good agreement with the neoclassical prediction, as illustrated in Fig. 15. This further confirms that the heat transport within the transport barrier is controlled by neoclassical transport processes and the loss power is dependent on the local plasma parameters at the edge transport barrier.

It should be mentioned that Fig. 15 only shows a few of the best hot ion discharges because TRANSP analysis can only be carried out for a limited number of cases. However, a survey of large numbers of hot ion discharges using a rough estimation for the loss power,

$$P_{NBI} - P_{\text{shinethrough}} - dW_{dia}/dt - P_{rad,core}$$

supports the above findings [34].

6. Summary and conclusions

Systematic variations in the edge pressure are observed between DD and DT hot ion H modes on
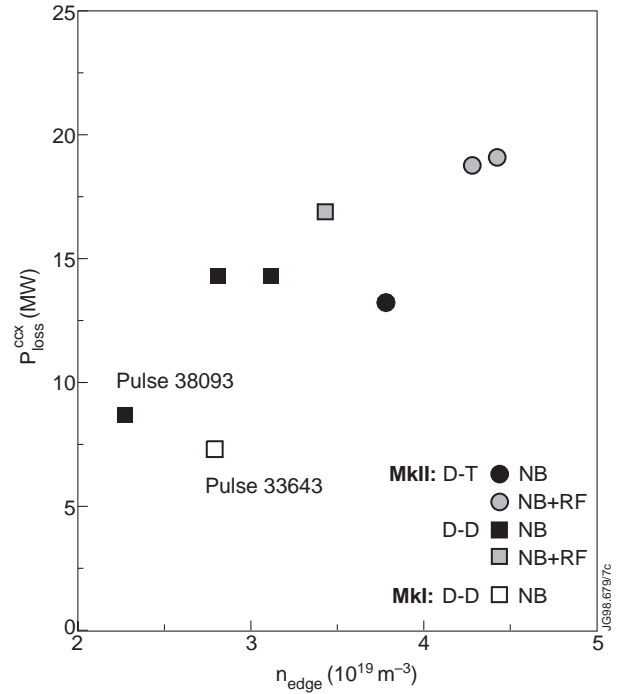

Figure 14. P_{loss}^{ccx} plotted against n_{edge} for the high performance hot ion H modes from Mark I and Mark II at 3.8 MA/3.4 T and 4.2 MA/3.8 T with $P_{NBI} = 18$–22 MW, $P_{ICRH} = 0$–3 MW. The data are taken close to the peak performance.

JET. For a given plasma current and magnetic configuration, DT discharges show a higher edge pressure immediately prior to the giant ELM which terminates the high performance phase, than seen in DD discharges. This has been shown for both the low power experiments used to demonstrate alpha heating and the full power high fusion performance plasmas in this regime. The effect can be as large as 25% and is more than twice the uncertainty in the measurements. The effect cannot be explained by shot to shot reproducibility, variations in recycling or MHD activity. It is clear therefore that there is an isotopic effect.

A higher pedestal is also observed for the injection of pure tritium beams into deuterium plasmas and for mixed DT beams into deuterium plasmas compared with that observed either for deuterium beams into deuterium plasmas or deuterium beams into DT plasmas. For the case of the injection of 25% tritium beams into either deuterium or DT plasmas the observed pedestal pressure is similar to that observed for pure deuterium beams into pure deuterium plasmas. Thus, the isotopic effect appears to
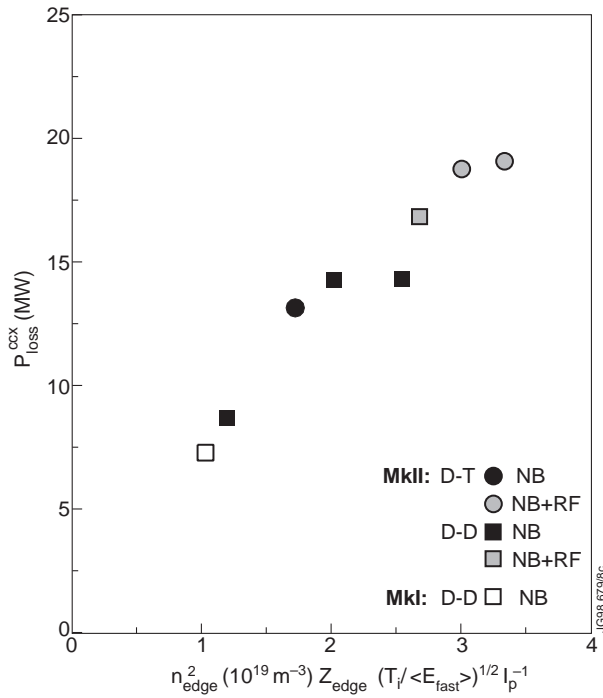
Figure 15. P_{loss}^{ccx} plotted against $n_{edge}^2 Z_{eff,edge} I_p^{-1}$ $\times \sqrt{T_i/\langle E_{fast}\rangle}$ for the high performance hot ion H modes from Mark I and Mark II (the same discharges as shown in Fig. 14).

be associated with the beam species, provided that a sufficient number of fast particles is present.

Heuristic models for the pedestal height have been proposed and used to explore a large data set of hot ion H mode plasmas. This analysis reveals that there is a clear scaling of pedestal height with plasma current, consistent with a pedestal width determined by a poloidal ion gyroradius. The thermal gyroradius model provides an adequate description of the data but would indicate that other sources of error or variation are affecting the data. Such a model ascribes some of the observed difference in pedestal pressure between DD and DT plasmas to the variations in ion temperature. Whilst the model cannot be unambiguously excluded, it does not fully account for the difference in measured pedestal pressure between high power DD and DT plasmas. The average fast particle model describes much of the data very well, but predicts that the highest pedestal should be found for pure tritium beam injection, which is at variance with the observations presented. The best description of the data is provided by a model where the barrier width is governed by the injected species with the largest gyroradius. For this model the scatter of the experimental measurements is consistent with

that expected from the measurement uncertainties, which would indicate that the plasma behaviour is very reproducible once the effects of MHD kink activity are eliminated. The model describes very well the observed variation of pedestal pressure with beam species provided that the fast ion density of the dominant species exceeds the order of 1%, as expected theoretically. As the plasma density is raised and the fast ion density falls it would be expected that fast ion effects cease to dominate and this is in line with the JET observations presented in Ref. [33], where it is found that at high edge density the thermal model provides the best description of those data.

It should be apparent from the discussion presented in this article that there is fairly compelling, but circumstantial, evidence for the role of fast particles in determining the transport barrier width. The effects are not so large compared with experimental uncertainties, and it has been necessary to examine the data rather carefully to reveal the underlying trends. It is to be hoped that the evidence presented in this article provides the stimulus for further experiments aimed at a definitive demonstration of the role of fast particles.

On the basis of the width scaling of the ion banana width of either thermal or fast particles, the power losses through the edge transport barrier are predicted by neoclassical theory to scale as $P_{loss} \propto n_{edge}^2 Z_{eff,edge} I_p^{-1}$, suggesting that the loss power is dependent on the local plasma parameters at the edge transport barrier. It has been demonstrated that this prediction is consistent with the experimental data from both the Mark I and Mark II divertors. However, a systematic increase in the loss power has been observed between the two divertor campaigns. In going from the Mark I divertor to the Mark II divertor, the loss power is increased significantly at similar edge densities. The carbon source from the Mark II divertor is actually about a factor of 2 higher than that in the Mark I divertor, which is attributed to the enhancement of chemical sputtering at the Mark II divertor target due to the higher base temperature of the target plate [30, 31]. This results in a significant increase in Z_{eff} at the edge in Mark II for the hot ion H modes, where the divertor shielding for impurities is poor, leading to the higher loss power in Mark II. In addition, with the more closed Mark II divertor, the divertor pumping for the recycling neutrals is strong and the central plasma density rise is slow, so that additional gas fuelling is necessary to optimize the fusion performance. However, the gas fuelling also affects

the recycling and hence increases the edge plasma density, thus aggravating the power losses in Mark II.

Acknowledgements

References

[1] Keilhacker, M., et al., Nucl. Fusion **39** (1998) 209.

[2] Thomas, P., et al., Phys. Rev. Lett. **80** (1998) 5548.

[3] JET Team (presented by P.J. Lomas), in Plasma Physics and Controlled Nuclear Fusion Research 1994 (Proc. 15th Int. Conf. Seville, 1994), Vol. 1, IAEA, Vienna (1995) 211.

[4] JET Team (presented by P.J. Lomas), in Fusion Energy 1996 (Proc. 16th Int. Conf. Montreal, 1996), Vol. 1, IAEA, Vienna (1997) 239.

[5] Wagner, F., et al., Phys. Rev. Lett. **53** (1984) 1453.

[6] Parail, V.V., et al., in Plasma Physics and Controlled Nuclear Fusion Research 1994 (Proc. 15th Int. Conf. Seville, 1994), Vol. 1, IAEA, Vienna (1995) 255.

[7] Cherubini, A., et al., Plasma Phys. Control. Fusion **38** (1996) 1421.

[8] Shaing, K.C., Crume, E.C., Jr., Phys. Rev. Lett. **63** (1989) 2369.

[9] Diamond, P.H., Kim, Y.B., Phys. Fluids B **3** (1991) 1626.

[10] Romanelli, F., Zonca, F., Phys. Fluids B **5** (1993) 4081.

[11] Bhatnager, V.P., et al., Nucl. Fusion **39** (1999) 353.

[12] Connor, J.W., Wilson, H.R., Plasma Physics Note 97/4.1, UKAEA Fusion, Culham (1997).

[13] Coppi, B., et al., Phys. Fluids B **2** (1990) 927.

[14] Pogutse, O., et al., in Controlled Fusion and Plasma Physics (Proc. 24th Eur. Conf. Berchtesgaden, 1997), Vol. 21A, Part III, European Physical Society, Geneva (1997) 1041.

[15] Porchelli, F., Rosenbluth, M.N., Plasma Phys. Control. Fusion **40** (1998) 481.

[16] Hinton, F.L., Staebler, G.M., Phys. Fluids **5** (1993) 1281.

[17] Parail, V.V., Guo, H.Y., Lingertat, J., Nucl. Fusion **39** (1999) 369.

[18] Huysmans, G.T.A., et al., in Controlled Fusion and Plasma Physics (Proc. 22nd Eur. Conf. Bournemouth, 1995), Vol. 19C, Part I, European Physical Society, Geneva (1995) 201.

[19] Nave, M.F.F., et al., Nucl. Fusion **37** (1997) 809.

[20] Doyle, E., et al., Phys. Fluids B **3** (1991) 2300.

[21] Connor, J.W., Plasma Phys. Control. Fusion **40** (1998) 531.

[22] Gohil, P., et al., Phys. Rev. Lett. **61** (1988) 1603.

[23] Zohm, H., Plasma Phys. Control. Fusion **38** (1996) 105.

[24] Nave, M.F.F., et al., in Controlled Fusion and Plasma Physics (Proc. 24th Eur. Conf. Berchtesgaden, 1997), Vol. 21A, Part I, European Physical Society, Geneva (1997) 1.

[25] Nave, M.F.F., et al., Nucl. Fusion **39** (1999) 1567.

[26] von Hellermann, M.G., et al., in Diagnostics for Experimental Thermonuclear Fusion Reactors (Stott, P.E., Gorini, G., Sindoni, E., Eds), Plenum Press, New York and London (1996) 281.

[27] Marcus, F.B., et al., Nucl. Fusion **37** (1997) 1067.

[28] Lingertat, J., et al., J. Nucl. Mater. **266–269** (1999) 124.

[29] JET Team (presented by A. Taroni), in Fusion Energy 1996 (Proc. 16th Int. Conf. Montreal, 1996), Vol. 2, IAEA, Vienna (1997) 477.

[30] Breger, P., et al., in Controlled Fusion and Plasma Physics (Proc. 24th Eur. Conf. Berchtesgaden, 1997), Vol. 21A, Part I, European Physical Society, Geneva (1997) 69.

[31] Wesson, J., Tokamaks, Clarendon Press, Oxford (1987).

[32] Rimini, F.G., et al., Nucl. Fusion **39** (1999) 1591.

[33] Saibene, G., et al., Nucl. Fusion **39** (1999) 1133.

[34] Guo, H.Y., et al., J. Nucl. Mater. **266–269** (1999) 825.

[35] Guo, H.Y., et al., "Effect of divertor geometry and chemical sputtering on impurity behaviour and plasma performance in JET", submitted to Nucl. Fusion.

[36] Matthews, G.F., et al., J. Nucl. Mater. **196–198** (1992) 374.

[37] McCracken, G.M., et al., Nucl. Fusion **39** (1999) 41.

[38] Simonini, R., et al., Contrib. Plasma Phys. **34** (1994) 368.